Available online at www.sciencedirect.com
SCIENCE DIRECT®
Journal of Solid State Chemistry 179 (2006) 308–314
JOURNAL OF SOLID STATE CHEMISTRY
www.elsevier.com/locate/jssc

Preparation and characterization of $LiNi_{0.8}Co_{0.2}O_2$/PANI microcomposite electrode materials under assisted ultrasonic irradiation

Y. Mosqueda[a], E. Pérez-Cappe[a], J. Arana[b], E. Longo[b], A. Ries[b], M. Cilense[b], P.A.P. Nascente[c], P. Aranda[d], E. Ruiz-Hitzky[d,*]

[a]*Laboratory of Chemistry of Materials-IMRE, Havana University, Havana, Cuba*
[b]*Chemistry Department, UNESP, Araraquara, Brazil*
[c]*CCDM-Universidade de Sao Carlos, Brazil*
[d]*Instituto de Ciencia de Materiales de Madrid, CSIC, Cantoblanco E-28049, Madrid, Spain*

Received 25 April 2005; received in revised form 12 September 2005; accepted 17 September 2005
Available online 2 November 2005

Abstract

A preparation method for a new electrode material based on the $LiNi_{0.8}Co_{0.2}O_2$/polyaniline (PANI) composite is reported. This material is prepared by in situ polymerization of aniline in the presence of $LiNi_{0.8}Co_{0.2}O_2$ assisted by ultrasonic irradiation. The materials are characterized by XRD, TG-DTA, FTIR, XPS, SEM-EDX, AFM, nitrogen adsorption (BET surface area) and electrical conductivity measurements. PANI in the emeraldine salt form interacts with metal-oxide particles to assure good connectivity. The dc electrical conductivity measurements at room temperature indicate that conductivity values are one order of magnitude higher in the composite than in the oxide alone. This behavior determines better reversibility for Li-insertion in charge–discharge cycles compared to the pristine mixed oxide when used as electrode of lithium batteries.

Keywords: PANI; Ni–Co mixed oxides; Organic–inorganic composites; Electrode materials; Lithium batteries

1. Introduction

The Ni-rich oxides of the Li–Ni–Co system present characteristics such as high cell voltage, high and variable oxidation states, high electronic conductivity at room temperature, making them interesting for applications as electrode in rechargeable lithium batteries [1–4]. However, their commercialization is currently limited due to structural impediments associated with the cationic disorder in the octahedral layer occupation [5–7]. Among different synthetic strategies proposed as alternatives to overcome such limitations, we have recently proposed a chemical method for preparation of a Ni-rich mixed oxide phase with structural cationic ordering that enhances its behavior as lithium battery positive electrode [8]. On the other hand, it is known that Ni–Co mixed oxides present a close packed crystalline structure in which octahedral sites are occupied by lithium ions. As the structural features of these materials negatively influence lithium diffusion, their use as battery cathodes imposes one to work at low current (typically 30–50 μA). In addition, these oxides have high relative density and very poor mechanical properties making them less attractive for practical purposes.

To overcome the above problems we aim to contribute preparing hybrid materials of the $LiNi_{0.8}Co_{0.2}O_2$ nickel-rich phase combined with a classic conducting polymer such as polyaniline (PANI). Doped PANIs are conducting materials of interest for use in secondary batteries [9,10] that have been also satisfactorily combined with inorganic redox oxides, giving systems suitable for electrochemical Li intercalation. The first PANI-based nanocomposite was reported by Kanatzidis and co-workers [11]. These authors described the intercalative polymerization of aniline in V_2O_5 xerogel giving PANI-nanocomposites of good electrical conductivity. Later on Nazar and co-workers demonstrated the feasibility of these materials for reversible electrochemical lithium insertion and therefore their

*Corresponding author. Fax: +34 91 372 06 23.
E-mail address: eduardo@icmm.csic.es (E. Ruiz-Hitzky).

0022-4596/$ - see front matter © 2005 Elsevier Inc. All rights reserved.
doi:10.1016/j.jssc.2005.09.030

applicability as electrodes for rechargeable lithium batteries [12,13]. The lithium chemical diffusion coefficient is higher for the nanocomposite than for the oxide alone by one order of magnitude, this effect being particularly remarkable for high cycling rates [13]. On the basis of this approach, the development of conducting nanocomposites received significant attention, deserving new studies using other polymers combined at the molecular (nanometer) level with different inorganic solids [14–17]. Many of these systems involve inorganic hosts exhibiting a layered structure susceptible to be exfoliated by the guest polymer intercalation. Non-intercalable and three-dimensional structured metal oxides could be also combined with conducting polymers such as PANI or polypyrrole (PPy) giving rise to the so-called microcomposites, i.e. materials combined at the micrometer scale, or even nanocomposites taking into account the micrometer or nanometer scale size of the involved oxide particles [18–22]. The resulting solids can exhibit better electrical, electrochemical, mechanical, morphological and thermal properties than the former components (inorganic solid and guest polymeric species) and some of them have been also tested in rechargeable lithium batteries applications [23–25]. Concerning Ni and Co dioxides/PANI systems, Ramachandran and co-workers [26] have reported PANI intercalation by previous treatment of the host solids with ammonium peroxodisulfate. As discussed below, the same method applied to $Li_xNi_{0.8}Co_{0.2}O_2$ phases does not produce intercalation compounds.

As sonochemistry appears as a powerful tool for preparation of a great variety of materials [27] this strategy has been applied here to prepare PANI/$LiNi_{0.8}Co_{0.2}O_2$ composites by polymerization of PANI in the presence of $LiNi_{0.8}Co_{0.2}O_2$ as a microparticulated solid assisted by ultrasound irradiation. This type of approach has been recently applied to the preparation of comparable materials, for instance, PANI/TiO_2 composites providing compounds of enhanced conductivity, e.g. $\sigma = 0.72\,S\,cm^{-1}$ at room temperature [28]. The final objective of the present work is to prepare electroactive PANI/$LiNi_{0.8}Co_{0.2}O_2$ microcomposites showing enhanced electrical conductivity and preserving their reversible electrochemical Li-insertion behavior, which make them improved electrode materials for Li-rechargeable batteries.

2. Experimental section

2.1. Synthesis

$LiNi_{0.8}Co_{0.2}O_2$ is synthesized by a procedure previously described following a Li–Ni–Co mixed citrate route for the preparation of the $Li_{0.7}Ni_{0.8}Co_{0.2}O_2$ phase [8] that has been modified in the present case to reach the desired stoichiometry. In this way, the thermal decomposition of the citrate precursor has been carried out here in sealed Au crucibles adding 0.3 mole/formula of $LiOH \cdot H_2O$ to procure additional Li. The $LiNi_{0.8}Co_{0.2}O_2$/PANI composite (1:1 oxide/polymer intended ratio) was prepared from 200 mg of the mixed oxide, 100 mg of anilinium chloride, 220 mg of ammonium peroxodisulfate (1:1 monomer/oxidant molar ratio) and, 1.5 g of sodium lauryl sulfate (surfactant). The starting reagents were dispersed in 200 ml of 1.5 M HCl and the mixture sonicated 1 h using a Sonics ultrasonic liquid processor (600 W) with a probe working at 240 KHz. The experiments were carried out at room temperature in air atmosphere. The resulting colloidal dispersion was flocculated with absolute ethanol and first washed three times with 100 mL of 0.2 M HCl to remove residual monomer, oxidant, and its decomposition products, and then with acetone to eliminate low-molecular-weight organic intermediates and oligomers. The ultrafine powder composite was vacuum dried at 60 °C. For comparative purposes, bulk PANI was synthesized following the same procedure.

2.2. Characterization

X-ray diffraction patterns (XRD) were registered with a Rigaku ultra-X 18BV2, (CuK_α radiation, 42 kV, 120 mA) at a step scan rate of 0.02°/s in the 10–120° 2θ range. X-ray photoelectron spectroscopy (XPS) was carried out using a XSAMHS surface spectramicroscopy with an Al K_α X-ray source at 1486.6 eV energy and 140 W power. The binding energy of the core level C_{1s} was set at 284.8 eV. Deconvolution of peaks into their components was carried out with software provided by the furnisher consisting of a Gaussian line shape Lorentzian function on a Shirley background. The surface elemental compositions were determined from the ratio of the peak areas corrected with the empiric sensitivity factors. The TG curves were obtained in static air atmosphere using a Netzsch-Thermische analyzer equipped with a PU1.851.01 unit power and a TASC 414/2 controller, using as reference α-Al_2O_3 and a Pt/Pt–Rh 10% thermocouple. The IR spectra were registered with a Perkin Elmer 567 model spectrophotometer, in the 400–4500 cm^{-1} wave number range; the solid samples were diluted in KBr pellets. The SEM-EDX and the atomic force microscopy (AFM) micrographs were carried out on a Princeton Gamma-Tech.Inc equipment, SM300 model provided by TOPCON and a Multimode TM Scanning probe microscope MMAFM-2 model of Digital Instruments, respectively. Samples (powders) were Au sputtered for the SEM study. The four-point conductivity measurements at room temperature were carried out using a homemade apparatus described elsewhere [29], the samples being in the form of pellets (0.33 cm^2 area, 0.05 cm thickness) pressed at 7 ton/cm^2.

Electrochemical measurements were conducted in Li/$LiClO_4$ (PC:EC)/($LiNi_{0.8}Co_{0.2}O_2$/PANI) and Li/$LiClO_4$ (PC:EC)/[$LiNi_{0.8}Co_{0.2}O_2$/carbon black (10%)] cells. The positive electrode was prepared as pellets of 0.13 cm diameter using 0.5 g of either the microcomposite or the pristine oxide (with 10% carbon black) pressed at 3 ton/cm^2 and heated at 100 °C for 4 h. The cells, assembled

into an argon-filled dry box, were galvanostatically cycled under 100 and 30 μA, respectively, of direct current in the 3–3.8 V voltage range.

3. Results and discussion

In a first set of experiments we have applied the procedure reported by Ramachandran et al. [26] trying to prepare PANI/$LiNi_{0.8}Co_{0.2}O_2$ composites with the aim to obtain nanocomposites based on the in situ intercalative polymerization of PANI within the mixed oxide layers. It should be remarked that although this last procedure was apparently successfully applied to obtain intercalation compounds of related solids, such as $LiNiO_2$ and $LiCoO_2$ [26], in our case the resulting compounds consisted of a mixture of scarce homogeneity formed by PANI and the starting mixed oxide without intercalation.

We have instead tested alternative strategies with the objective to prepare composites without exfoliation of the mixed oxide but in which the $LiNi_{0.8}Co_{0.2}O_2$ was present as a microparticulated solid. In this way, PANI/$LiNi_{0.8}Co_{0.2}O_2$ microcomposites have been prepared by treatment of a mixture of $LiNi_{0.8}Co_{0.2}O_2$ synthesized from the citrate route [8] and anilinium chloride under ultrasound irradiation. To assure the formation of PANI in its emeraldine salt form the treatment was carried out in the presence of $(NH_4)_2S_2O_8$ in acid media (aq. HCl). The resulting material consists of a polymer/mixed oxide microcomposite with an almost 1:1 (w/w) ratio as deduced from the TG analyses (polymer loss of about 50% in weight) (Fig. 1). The weight loss up to about 600 °C observed in the TG curve of the microcomposite shows a similar trend than that observed for bulk PANI. The first weight loss between 50 and 100 °C is associated with the removal of physically adsorbed water molecules. This weight loss represents 0.3% and 10% of total weight for the composite and PANI, respectively. The water content is related to the hygroscopic character of the conducting polymer and must be borne in mind for lithium battery applications. It should be noted that alternative methods to combine the polymer and the oxide, e.g. magnetic stirring instead sonication, give materials showing lower homogeneity with almost similar conductivity values than the pristine oxide alone.

The XRD patterns of $LiNi_{0.8}Co_{0.2}O_2$ pristine oxide, oxide/PANI microcomposite and bulk PANI are shown in Fig. 2. The diagram of the microcomposite shows the coexistence of reflections related to both $LiNi_{0.8}Co_{0.2}O_2$ and PANI, although the low crystallinity of the polymer produces high scattering that may hide some characteristic diffraction peaks of the mixed oxide. The preservation of $LiNi_{0.8}Co_{0.2}O_2$ crystallinity is verified by TEM showing nanometric oxide particles embedded in the polymer matrix. Enlargement of XRD peaks of the oxide can be explained by the diminution of its particle size as consequence of the ultrasound irradiation. The three characteristic diffraction peaks centered at 0.54, 0.44 and 0.35 nm (16.5, 20.1 and 25.1 $2\theta^{\circ}$) corresponding to PANI in its emeraldine salt form [28,30,31], are present in the bulk PANI and the PANI/$LiNi_{0.8}Co_{0.2}O_2$ microcomposite both prepared by sonication. The peak at 0.44 nm attributed to the (100) reflection is slightly more intense than that at 0.35 nm corresponding to the (110) reflection. According to Pouget and co-workers [30] the relative intensities of both reflections are very sensitive to the ring tilt angle and to the Cl–N distance indicating a similar structure of bulk PANI and PANI/$LiNi_{0.8}Co_{0.2}O_2$ microcomposite. This behavior is different from the PANI/TiO_2 composites prepared by sonication by Xia and Wang [28], probably being related to a lower doping level of the emeraldine salt in the present case as the synthesis has been carried out in a less concentrated HCl medium.

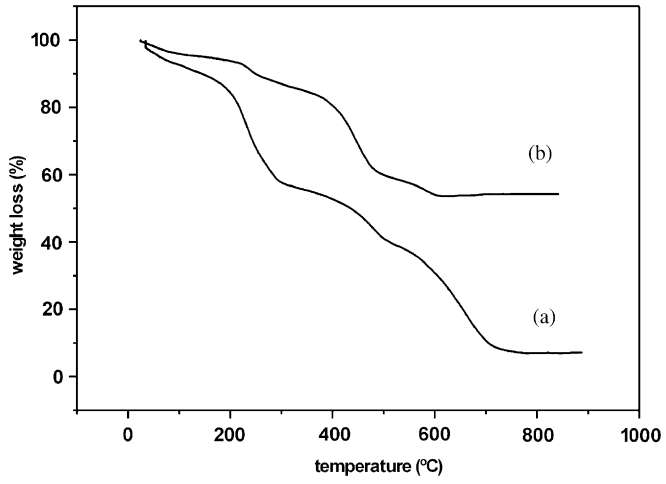

Fig. 1. TG curves of bulk PANI (a) and PANI/$LiNi_{0.8}Co_{0.2}O_2$ microcomposite (b).

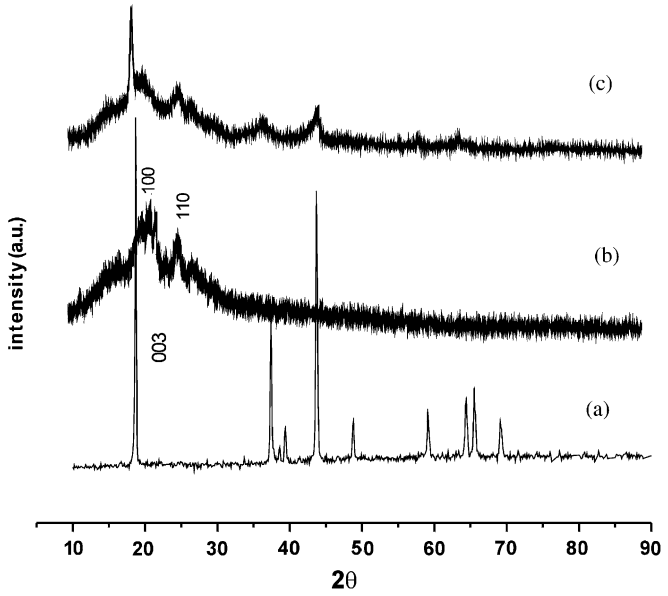

Fig. 2. XRD patterns of pristine $LiNi_{0.8}Co_{0.2}O_2$ oxide (a), bulk PANI (b) and PANI/$LiNi_{0.8}Co_{0.2}O_2$ microcomposite (c).

Fig. 3 shows the IR spectra (400–2000 cm^{-1}) of both the bulk PANI and the PANI/$LiNi_{0.8}Co_{0.2}O_2$ microcomposite. In bulk PANI, the bands assigned to benzoid (B) and quinoid (Q) ring deformations appear at 1467 and 1549 cm^{-1}, respectively. Both bands shift to higher wave number (1492 and 1575 cm^{-1}, respectively) in the microcomposite reversing their relative intensities. This observation indicates that Q rings predominate in the polymer formed in the microcomposite compared to bulk PANI, suggesting a higher oxidation degree in the polymer backbone of the former due to its interaction with the surface of the mixed oxide. The wave number shift is also consistent with a lower degree of PANI protonation in the microcomposite, which is confirmed by a similar shift effect observed for the bands in the 1400–1100 cm^{-1} region [32]. The bands around 800 and 1010–1170 cm^{-1} are assigned to C–H out-of-plane and in-plain bending modes, respectively, characteristic of *p*-di-substitution in benzene rings. The band corresponding to the CH out-of-plane bending vibration mode of mono-substituted benzene ring is not observed, indicating that the degree of polymerization is large. This interpretation is also supported by the observation in both materials of a band around 1300 cm^{-1}, which is usually associated with C–N stretching vibrations of secondary aromatic amine groups [33].

The band at 1232 cm^{-1} can be assigned to C–N stretching vibrations of benzenoid species. Some authors have interpreted it as originating from a bipolaron structure, which could be related to the conducting form of PANI [34,35]. The 1135 cm^{-1} band observed in the microcomposite, which is considered as an "electronic band" associated with conduction in doped PANI [33,35,36], can be assigned to a vibration mode of $-NH^+=$ (semiquinone radical cation, $IP^{\bullet+}$) structures [31,37]. It should be expected that the oxide surface strongly interacts with the conjugate structure of PANI, especially through the quinoid ring (semiquinone radical cation), as it has been reported in other systems [28,38]. The observed low slope in the IR spectrum above 2000 cm^{-1} is indicative of a low protonation degree which is directly related to the experimental conditions adopted in this work as above indicated. Finally, IR absorption bands appearing in the 3000–3500 cm^{-1} range are mainly assigned to stretching N–H vibrations in different environments.

By comparing the XPS spectra (Fig. 4) of pristine mixed oxide and PANI/oxide microcomposite a slight shift of binding energies for all the detected elements is observed, indicating a change of environment that affects all the involved atoms. It is noteworthy that both Ni and Co atoms located at the surface of the oxide particles in the microcomposite preserve their +3 oxidation state.

Using a fitting procedure that assumes Gaussian functions for describing N(1s) and C(1s) photoelectron lines as separate components in the XPS spectrum of the PANI/oxide microcomposite, the quantitative analysis summarized in Table 1 is proposed [36,39,40]. The existence of N^+ species and the lower peak area of NH^+ and/or NH_2^+ groups in relation to NH groups agree with the results obtained by IR and XRD techniques, meaning that a poorly doped emeraldine salt is formed in the presence of the mixed oxide. The high N^+ binding energy observed in the spectrum of the microcomposite is related not only to the interaction between this group and protons introduced

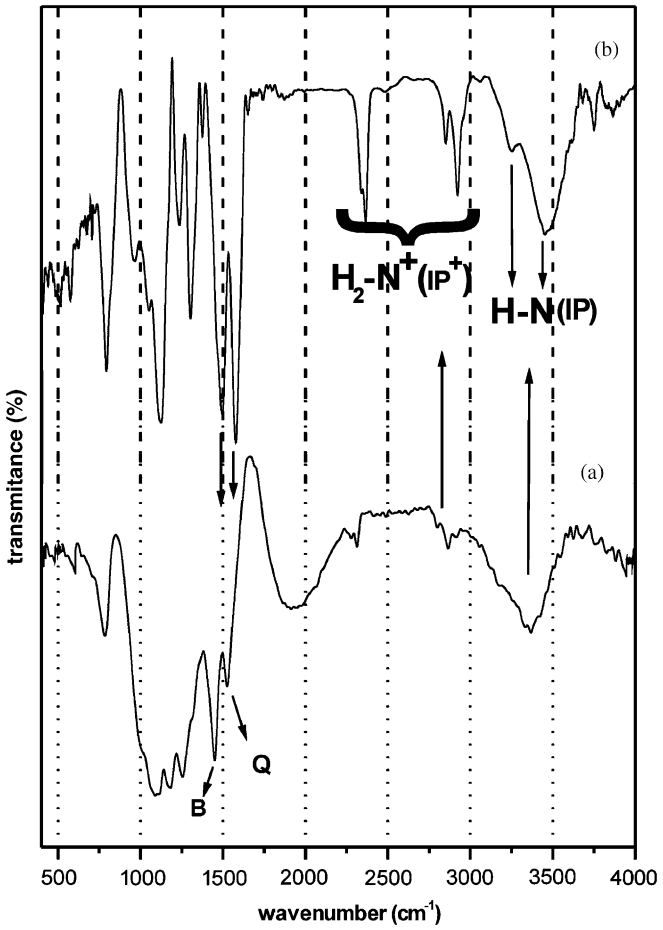

Fig. 3. IR spectra in the 400–2000 cm^{-1} range of bulk PANI (a) and PANI/$LiNi_{0.8}Co_{0.2}O_2$ microcomposite (b). B and Q represent the benzoid and quinoid rings of PANI.

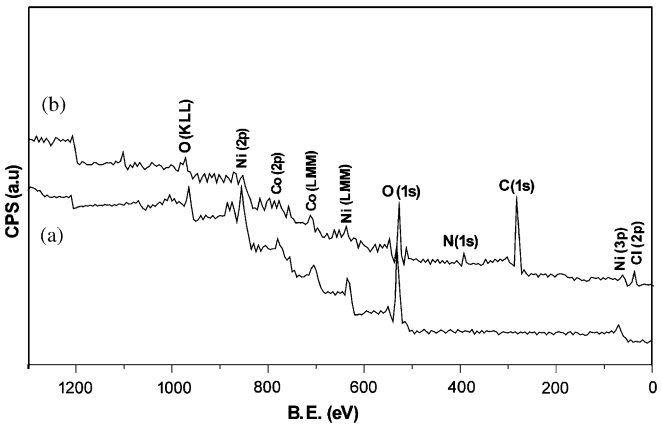

Fig. 4. XPS spectra of the pristine mixed oxide (a) and PANI/$LiNi_{0.8}Co_{0.2}O_2$ microcomposite (b).

by the acid dopant but also to the possible interaction with oxygen species on the oxide surface through charge-transfer-bridge, as reported by other systems [41,42].

Table 2 shows the surface atomic concentration in both pristine oxide and the PANI/$LiNi_{0.8}Co_{0.2}O_2$ microcomposite, calculated from XPS peak areas ratios and corrected by the empirical sensitivity factors. The Ni/N atomic concentration ratio in the PANI/$LiNi_{0.8}Co_{0.2}O_2$ microcomposite is 0.69, which is close to the theoretical value of 0.8 corresponding to a full coverage of the oxide particles. Preliminary results from electrophoretic mobility of bulk PANI, oxide particles and the resulting microcomposite support this interpretation.

Complementary information about the extent of contact between the oxide and the polymer in the composite is obtained from SEM-EDX and AFM analyses. A selected SEM microphotography representative of the microcomposite material is shown in Fig. 5a. The image reveals different textures in the material indicated by A, B, C and D. Thus, the nature of the microcomposite can be explained as a distribution of nanometric oxide particles embedded in the polymer matrix (regions C and D) coexisting with oxide particle of bigger size (A) surrounded by a thin skin of polymer in contact either with other particles or with the polymer matrix (the border indicated as B in the Fig. 5a). Energy dispersive X-ray analysis of

Table 1
Contribution of nitrogen and carbon peaks resulting from the fitting of Gaussian components to the C(1s) and N(1s) photoelectron spectra for the PANI/$LiNi_{0.8}Co_{0.2}O_2$ composite

Core-level	Group	Binding energy (eV)	Peak area (%)
C(1s)	C–C, C–H	284.6	64
	C–N, C=N	286.3	27
	$C–N^+$, $C=N^+$, C=O	287.6	9
N(1s)	NH, N=C	399.5	79
	NH^+(polaron), NH_2^+ (bipolaron)	401.8	21

Table 2
Surface atomic concentration in both oxide pristine and PANI/$LiNi_{0.8}Co_{0.2}O_2$ composite calculated from peak areas ratios

Sample	Atomic concentration (% atomic)					
	C	O	N	Cl	Ni	Co
Pristine oxide composite	—	13.3	—	—	14.9	4.3
	38.4	4.3	6.8	3.0	4.7	1.4

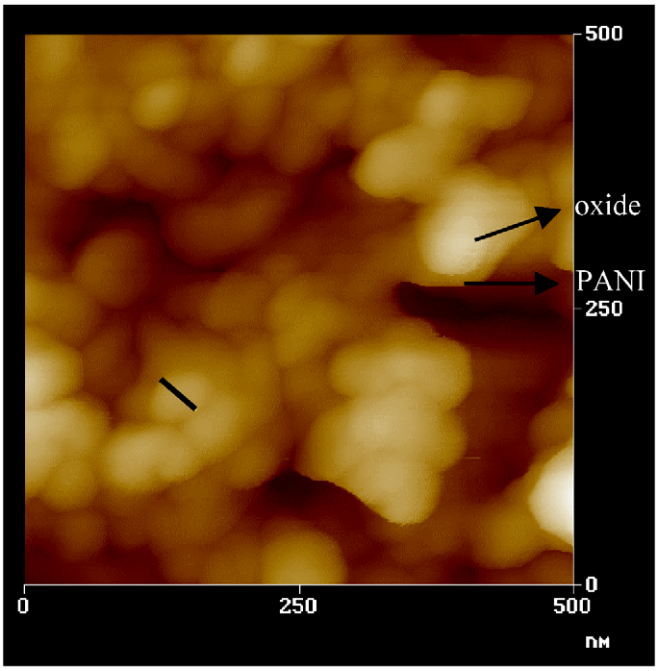

Fig. 6. AFM image of PANI/$LiNi_{0.8}Co_{0.2}O_2$ microcomposite corresponding to the C and D regions indicated in Fig. 5 (PANI/small oxide particles).

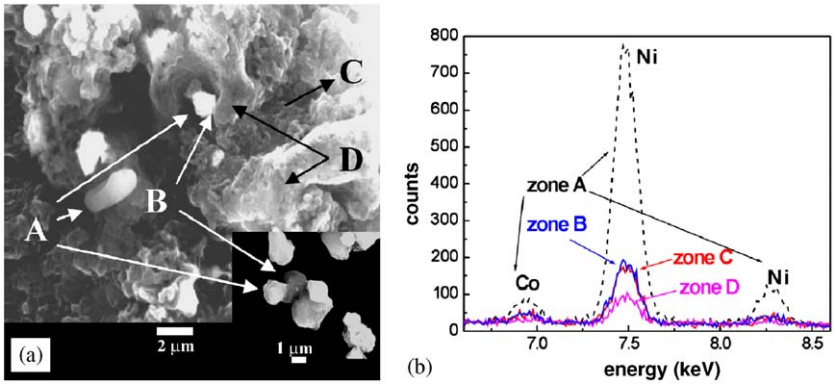

Fig. 5. (a) SEM micrographs of oxide/PANI microcomposite, showing some micrometric oxide particles (A) in contact (border indicated by B) with polymer-surrounded small oxide particles (C,D). The inset shows a detail of the contact between particles (A) that are cemented by PANI (border B); (b) EDX analysis of the different zones visualized in the SEM micrograph.

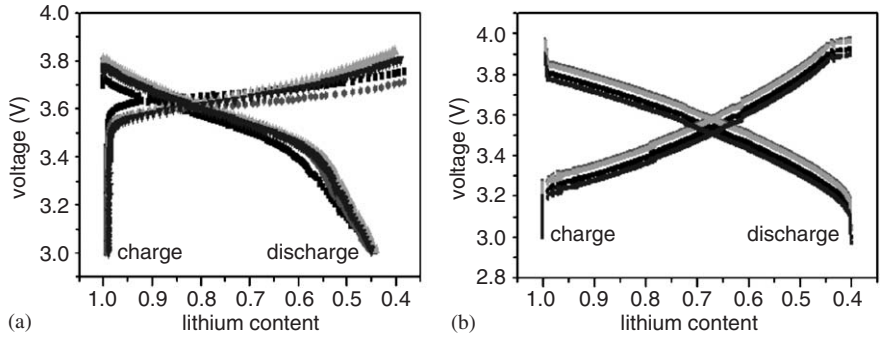

Fig. 7. Fourth and first charge–discharge cycles of Li/$LiClO_4$ (PC:EC)/($LiNi_{0.8}Co_{0.2}O_2$/carbon black) (a) and Li/$LiClO_4$ (PC:EC)/($LiNi_{0.8}Co_{0.2}O_2$/PANI) (b) electrochemical cells applying a current of 30 and 100 μA, respectively.

these different zones indicates different abundance of metal oxide (Fig. 5b) in each of the regions. The fact that the concentration of oxide nanoparticles in the polymer was variable in the different regions of the whole material can be a consequence of the existence of oxide particles of different size that submitted to the ultrasound treatment were non-homogenously dispersed in the bulk of the formed polymer. AFM (Fig. 6) shows oxide particles ($\approx$ 30 nm diameter) and PANI intimately combined. This image corroborates the connectivity among oxide particles provided by the polymer, which is of great significance in view of the electrical and electrochemical behavior of the microcomposite.

From dc conductivity measurements at room temperature determined by the Van der Paw's four-point method is deduced a value of 10^{-1} S cm^{-1} for the PANI/$LiNi_{0.8}Co_{0.2}O_2$ microcomposite. This conductivity is two orders of magnitude higher than that of the pristine $LiNi_{0.8}Co_{0.2}O_2$ alone or related oxide phases with lower content in lithium such as $Li_{0.7}Ni_{0.8}Co_{0.2}O_2$ [8]. The electrochemical behavior of the microcomposite when tested as electrode in a Li/$LiClO_4$ (PC:EC)/($LiNi_{0.8}Co_{0.2}O_2$/PANI) cell is shown in Fig. 7a, in which is represented the fourth and first charge–discharge cycles in the 3–3.8 V voltage range using a direct current of 100 μA. The electrochemical behavior of the Li/$LiClO_4$ (PC:EC)/($LiNi_{0.8}Co_{0.2}O_2$/carbon black) cell using a direct current of 30 μA is presented for comparison in Fig. 7b. It appears that the microcomposite works better as an electrode for lithium insertion–deinsertion compared to the pristine mixed oxide as it is possible to cycle the systems at higher current. This is agreement with the high diffusion coefficient (10^{-7} cm^2/s) of lithium determined by GITT measurements [43] and also with data already reported showing that conductive polymers enhance lithium diffusivity [13]. Moreover, recent investigations [33] indicate that lithium salt-doped PANI directly fabricated from solutions containing PANI and lithium salts, are more effectively doped than samples prepared by chemical treatment with protonic acid doping agents. It could be proposed that in a certain way the method used for preparing the composite may operate in an analogous way and may favor the increase of the amount of unpaired electrons (polarons) enhancing the conductivity of the system. This hypothesis is consistent with the existence of oxide–polymer interactions in the microcomposite.

4. Concluding remarks

Concerning the preparation of the $LiNi_{0.8}Co_{0.2}O_2$/PANI composites, the ultrasound treatment appears to be more effective than conventional methods, such as magnetic stirring, to produce more homogeneous materials containing a large amount of the metal oxide particles of small size. The composites prepared under these conditions can be regarded as microcomposites instead of nanocomposites in view of the size of most part of the oxide particles and the lack of intercalation/exfoliation of the metal oxide. PANI constitutes a matrix in which small particles of the oxide are embedded procuring connectivity in the system. The good contact between polymer and oxide particles determines the observed increase in the electrical conductivity of the microcomposite compared to the pristine oxide. The microcomposite maintains the Li-insertion ability of the oxide counterpart showing improved behavior as electrode for rechargeable lithium batteries as it is possible to perform the cycling at higher current values compared to the oxide with added carbon.

Acknowledgments

Financial support from the CSIC and the Havana University (CITMA) through a Spanish–Cuban cooperation (reference 2001CU0007), the CICYT (Spain, MAT2003-06003-C02-01 project) and the UNESP-MES cooperation are gratefully acknowledged.

References

[1] I. Saadoune, M. Ménétrier, C. Delmas, J. Mater. Chem. 12 (1997) 2505–2511.
[2] D.-W. Kim, Y.-K. Sun, Solid State Ionics 111 (1998) 243–252.
[3] C. Julien, L. El-Farh, S. Rangan, M. Massot, J. Sol–Gel Sci. Technol. 15 (1999) 63–72.
[4] J. Molenda, P. Wilk, J. Marzec, Solid State Ionics 119 (1999) 19–22.
[5] A. Rougier, I. Saadoune, P. Gravereau, P. Willman, C. Delmas, Solid State Ionics 90 (1996) 83–90.
[6] E. Zhecheva, R. Stoyanova, Solid State Ionics 66 (1993) 143–149.

[7] J. Morales, C. Pérez, J.L. Tirado, Mater. Res. Bull. 25 (1990) 623–625.
[8] Y. Mosqueda, E. Pérez-Cappe, P. Aranda, E. Ruiz-Hitzky, Eur. J. Inorg. Chem. (2005) 2698–2705.
[9] P. Nova, K. Müller, K. Santhanam, O. Haas, Chem. Rev. 97 (1997) 207–281.
[10] E. Genies, A. Syed, C. Tsintavis, Mol. Cryst. Liq. Cryst. 121 (1985) 181–186.
[11] M.G. Kanatzidis, C.-G. Wu, H.O. Marcy, C.R. Kannewurf, J. Am. Chem. Soc. 111 (1989) 4139–4141.
[12] F. Leroux, B.E. Koene, L.F. Nazar, J. Electrochem. Soc. 143 (1996) L181–L183.
[13] F. Leroux, G. Goward, W.P. Power, L.F. Nazar, J. Electrochem. Soc. 144 (1997) 3886–3895.
[14] E. Ruiz-Hitzky, Adv. Mater. 5 (1993) 334–340.
[15] E. Ruiz-Hitzky, P. Aranda, An. Quim. Int. Ed. 93 (1997) 197–212.
[16] P. Gómez-Romero, Adv. Mater. 13 (2001) 163–174.
[17] E. Ruiz-Hitzky, P. Aranda, in: T.J. Pinnavaia, G.W. Beall (Eds.), Polymer–Clay Nanocomposites, Wiley, West Sussex, 2000, pp. 19–46.
[18] S. Maeda, S.P. Armes, J. Coll. Interface Sci. 159 (1993) 257–259.
[19] R.F. de Farias, J.M. de Souza, J.V. de Melo, C. Airoldi, J. Coll. Interface Sci. 212 (1999) 123–129.
[20] B.Z. Tang, Y. Geng, J.W.Y. Lam, B. Li, X. Jing, X. Wang, F. Wang, A.B. Pakhomov, X.X. Zhang, Chem. Mater. 11 (1999) 1581–1589.
[21] H. Yoneyama, N. Takahashi, S. Kuwabata, J. Chem. Soc. Chem. Commun. (1992) 716–717.
[22] H. Yoneyama, A. Kishimoto, S. Kuwabata, J. Chem. Soc. Chem. Commun. (1991) 986–987.
[23] S. Kuwabata, A. Kisimito, T. Tanaka, H. Yoneyama, J. Electrochem. Soc. 141 (1994) 10–14.
[24] S. Kuwabata, T. Idzu, C.R. Martin, H. Yoneyama, J. Electrochem. Soc. 145 (1998) 2707–2712.
[25] S. Kuwabata, S. Masui, H. Tomiyori, H. Yoneyama, Electrochim. Acta 46 (2000) 91–97.
[26] K. Ramachandran, O. Christopher, M. Lerner, Mater. Res. Bull. 31 (1996) 767–772.
[27] D. Peters, J. Mater. Chem. 6 (1996) 1605–1618.
[28] H. Xia, Q. Wang, Chem. Mater. 14 (2002) 2158–2165.
[29] E. Pérez-Cappe, A. Villanueva, J.C. Gálvan, G. Pérez-Urrutia, E. Ruiz-Hitzky, Abstracts VI Reunión Nacional de Materiales, San Sebastián, Spain, 1999.
[30] J. Pouget, M. Josefowiez, A. Epstein, X. Tang, A.G. MacDiarmid, Macromolecules 24 (1991) 779–789.
[31] Y. Furukawa, T. Hara, Y. Hyodo, I. Harada, Synth. Met. 16 (1986) 189–198.
[32] S.-A. Chen, H.-T. Lee, Synth. Met. 47 (1992) 233–238.
[33] S.K. Ryu, B.W. Moon, J. Joo, S.H. Chang, Polymer 42 (2001) 9355–9360.
[34] J. Stejskal, I. Sapurina, M. Trchová, J. Prokeš, I. Křivka, E. Tobolková, Macromolecules 31 (1998) 2218–2222.
[35] S. Quillard, G. Louarn, S. Lefrant, A.G. MacDiarmid, Phys. Rev. B 50 (1994) 12496–12508.
[36] K.G. Neoh, E.T. Kang, K.L. Tan, J. Polym. Sci. Part B. Polym. Phys. 31 (1993) 395–401.
[37] Y. Furukawa, F. Ueda, Y. Hyodo, I. Harada, T. Nakajima, T. Kawagoe, Macromolecules 21 (1988) 1297–1305.
[38] J. Chen, Y. Zhang, D. Wang, H. Dai, J. Am. Chem. Soc. 123 (2001) 3838–3839.
[39] M.G. Han, S.S. Im, Polymer 41 (2000) 3253–3262.
[40] A.P. Monkmam, G.C. Steevens, D. Bloor, J. Phys. D: Appl. Phys. 24 (1991) 738–749.
[41] E.T. Kang, G.K. Neoh, K.L. Tang, Synth. Met. 68 (1995) 141–144.
[42] M. Cochet, W.K. Maser, A.M. Benito, M.A. Callejas, M.T. Martinez, J.M. Benoit, J. Schreiber, O. Chauvet, Chem. Commun. (2001) 1450–1451.
[43] Y. Mosqueda, Y. Rodríguez, E. Pérez-Cappe, J. Arana, E. Souza, Phys. Stat. Sol. C 2 (2005) 3774–3777.